

Photostable molecules on chip: integrated single photon sources for quantum technologies

P. E. Lombardi,^{†,‡,⊥} A. P. O'vvy, ^{¶,‡,⊥} S. Pazzagli,^{§,†} G. Mazzamuto,^{†,‡} G. Kewes,^{||} O. Neitzke,^{||} N. Gruhler,[¶] O. Benson,^{||} W.H.P. Pernice,[¶] F. S. Cataliotti,^{§,‡} and C. Toninelli^{*,†,‡}

CNR-INO, Istituto Nazionale di Ottica, Via Carrara 1, 50019 Sesto F.no, Firenze, Italy, LENS, Via Carrara 1, 50019 Sesto F.no, Firenze, Italy, Institute of Physics, University of Muenster, Muenster, Germany, Università di Firenze, Via Sansone 1, I-50019 Sesto F.no, Firenze, Italy, and Nano-Optik, Institut für Physik, Humboldt-Universität zu Berlin, Berlin, Germany

E-mail: toninelli@lens.unifi.it

KEYWORDS: Integrated quantum optics, PAH molecules, single photon sources, hybrid photonics

^{*}To whom correspondence should be addressed

[†]CNR-INO, Istituto Nazionale di Ottica, Via Carrara 1, 50019 Sesto F.no, Firenze, Italy

[‡]LENS, Via Carrara 1, 50019 Sesto F.no, Firenze, Italy

[¶]Institute of Physics, University of Muenster, Muenster, Germany

[§]Università di Firenze, Via Sansone 1, I-50019 Sesto F.no, Firenze, Italy

^{||}Nano-Optik, Institut für Physik, Humboldt-Universität zu Berlin, Berlin, Germany

[⊥]Contributed equally to this work

Abstract

The on-chip integration of quantum light sources and nonlinear elements poses a serious challenge to the development of a scalable platform for quantum information and communication. In this work we demonstrate the potential of a novel hybrid technology which combines single organic molecules as quantum emitters and dielectric chips, consisting of ridge waveguides and grating far-field couplers. Dibenzoterrylene molecules in thin anthracene crystals exhibit long-term photostability, easy fabrication methods and life-time limited emission at cryogenic temperatures. We couple such single emitters to silicon nitride ridge waveguide with a branching ratio of up to $40 \pm 3 \%$, considering both propagation directions. Single wave-guided photons can be readily processed on-chip or efficiently extracted into a quasi-gaussian mode in free space.

Many Quantum technologies substantially require efficient sources of non-classical light.^{1,2} In particular, bright, reliable sources of single photons are a basic ingredient for linear optical quantum computing protocols,³ boson sampling algorithms, secure quantum communications⁴ and quantum imaging.⁵ In this context, single quantum emitters (SQEs) under pulsed excitation have been proposed as deterministic sources of indistinguishable single photons.⁶ They represent an alternative route to heralded generation from parametric down conversion,⁷ insofar as decoherence and losses are suppressed. Enhancement and control of light-matter interfaces are hence crucial for the efficient collection and processing of the delivered photons. Under tight focusing in free space, total reflection from a single atom has been predicted,⁸ while single-molecule nonlinearity has been experimentally observed.⁹ Optical cavities help improving brightness and indistinguishability^{10–12} and allow for optical nonlinearity in the few photon regime.^{13,14} The nanoscale field confinement in dielectric and plasmonic antennas has been also put forward,¹⁵ allowing unidirectional emission,^{16,17} almost unitary collection efficiency¹⁸ and fast repetition rate.¹⁹ On the other hand, coupling SQEs to the evanescent field in tapered fibers is especially convenient for outcoupling.^{20,21} However, direct coupling of QEs to single mode waveguides (WGs) in a planar geometry is particularly favorable for the realization of integrated quantum optical circuits,^{22,23} enabling also logic operations^{24,25} and detection on the same physical platform. In this respect, a high branching ratio is attained in photonic-crystal WGs^{26,27} whereas on-chip ridge WGs^{28–30} allow for long-range propagation and direct signal processing.

Concerning QEs, among different types, including atoms, color centers in diamond and epitaxial quantum dots, single molecules of polyaromatic hydrocarbons have shown remarkable features,^{9,31} but only few works have claimed their integration in relevant photonic structures.^{32–34}

Here we demonstrate the emission of single photons from Dibenzoterrylene (DBT) molecules into ridge WGs with a branching ratio up to $40 \pm 3 \%$. Our approach builds on the advantages of an all-solid-state platform, such as miniaturization and scalability. Indeed nanoscale emitters are simply integrated by spin-coating onto the photonic chip, containing WGs and far-field couplers as sketched in Fig.1a. The overall single-photon source efficiency, including emission into the guided mode, propagation with 4.9-dB/cm losses,³⁵ and emission into a quasi-gaussian mode in free space is estimated around $16 \pm 1 \%$. These results are competitive with state-of-the-art single photon emission into guided modes from solid state systems,^{30,36} while offering a novel platform with unprecedented versatility. In particular, DBT molecules embedded in a rigid matrix of crystalline anthracene (Ac) show photostable emission both at room and at cryogenic temperatures. Compared to available emitters in solid state systems, it holds promise because of an almost unitary quantum yield and negligible blinking, limited by the intersystem crossing yield (10^{-7}) to the short-lived triplet state.^{37,38} At liquid helium temperature, these photons can be made indistinguishable with 30 % emission into the zero-zero phonon line, and are therefore well suited for carrying quantum information with high fidelity.³¹ This behavior is preserved also in crystals as thin as 50 nm, obtained by drop-casting anthracene-DBT in solu-

tion onto a rapidly spinning plate, thus enabling straight-forward integration in photonic chips (see SI). Notably, positioning QEs in the pronounced evanescent field attainable in tight single-mode ridge WGs has been proposed for efficient collection of single photons into guided modes.²⁸

Our optical chip consists of a square glass die, covered with a thin layer of silicon nitride (Si_3N_4). The nanophotonic circuits are then fabricated using three steps of electron-beam lithography, followed by reactive ion etching, yielding 175 nm-thick and 500 nm-wide single mode optical WGs. In order to couple light out of the WGs for detection in free space, we have developed a grating design, following the guidelines given in Ref.³⁹. Gratings are based on fully-etched rectangular elements, buried in a 760 nm-thick hydrogen silsequioxane (HSQ) buffer layer with a 120 nm-thick gold mirror on top, in order to enhance directionality. Finite elements simulations yield a value of up to 90% for the output coupling efficiency (c), (see SI). A typical white light image of the bare waveguide-couplers device is shown in the top panel of Fig.1b, where the gold mirrors highlight the coupler regions. The HSQ pads and the waveguide appear in dark grey. In order to characterize the grating couplers, we have optimized apodization and tapering length to fit a gaussian mode in free space. We can hence extract the outcoupling efficiency from transmission measurements, as depicted in the bottom panel of Fig.1b. Laser transmission at 785 nm is collected by the imaging system (Fig.1b middle panel), integrated over the coupler area and normalized to the reflection from a silver mirror (after background subtraction on both images). The single coupler efficiency is then evaluated as the square root of the throughput. Measured values yield $\eta_c = 35.0 \pm 0.5\%$. Results below expectations can be attributed to the non-optimal HSQ thickness in the fabricated chips (see SI). The transmission spectrum in Fig.1a shows the device bandwidth, which allows for efficient out-coupling also at room temperature, where the molecule emission spectrum is about 50-nm broad. The successful deposition of DBT-doped anthracene crystals on the chip can be appreciated from white light images, such as the one in the top panel of Fig.1c. Here just a tiny portion of the crystal covers the waveguide

central region. After spincoating highly diluted DBT-anthracene solution, around 40% of the devices contain crystals and among these, 1/3 shows fluorescing molecules close to the waveguide. As

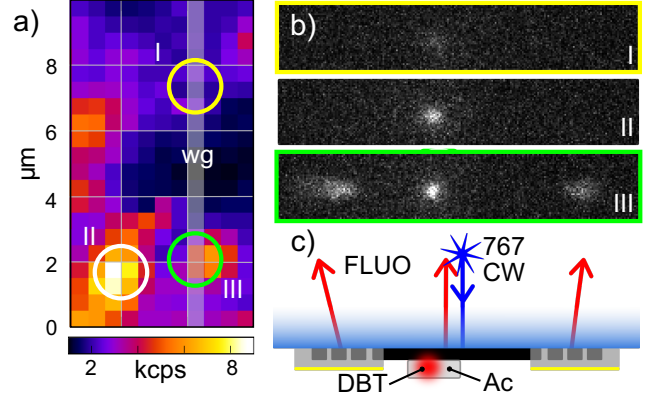


Figure 2: Guided fluorescence. a) Confocal fluorescence map from DBT:anthracene crystals, deposited on the chip around a waveguide region. b) EMCCD image of the fluorescence from the entire device when excited confocally in point I (no molecule on WG), II (molecule off guide) and III (WG-coupled molecule). The estimated coupling efficiency amounts to 40%. c) Cartoon for the experimental configuration.

a first evidence of DBT-WG coupling, we report in the middle panel of Fig.1c the device fluorescence imaged onto the electron multiplying charge coupled device (EMCCD), when the pump laser is coupled to the WG from the left side and filtered out before detection. Molecules in the vicinity of the WG are excited through the guided mode and exhibit fluorescence. The signal collected from the out-couplers contains though some residual laser light. In order to isolate the molecular emission, pump and fluorescence are further spatially separated by exciting each molecule with confocal illumination. The molecule distribution on the chip is first observed by scanning the sample under the confocal laser spot and measuring the fluorescence signal from the same position with a single photon avalanche diode (SPAD). An example of such a fluorescence map is displayed in Fig.2a, where the white-shaded rectangle indicates the underlying waveguide structure. In the three panels of Fig.2b the fluorescence spatial distribution from the entire device area is compared for a molecule sitting far (II), and in the near-field (III) of the

waveguide. Clearly, the output couplers light up if and only if a molecule is coupled to the waveguide, showing that direct scattering between the confocal fluorescence spot and the gratings is negligible. Panel (I) represents instead the background signal, obtained by illuminating an empty crystal on the WG. A small amount of laser leakage is present on the illumination point, but no signal is detected at the out-couplers.

The quantum nature of the WG-coupled light is captured in the measurements of the field second order autocorrelation function ($g^{(2)}(\tau)$), presented in Fig.3c and d. Here, coincidence counts are plotted for fluorescence photons collected either from the source position or from one coupler, corresponding to the area circled in the CCD image of Fig.3a. A fluorescence map relative to the same device is shown in Fig.3b. The experimental data for the $g^{(2)}(\tau)$ (black circles) are presented without background subtraction and show good agreement with the fitting function $g^{(2)}(\tau) = 1 - b\exp(\tau/T)$ (red solid line). Clear evidence of single photon emission is obtained in both cases: $g^{(2)}(0) = 0.33 \pm 0.09$ when collecting directly from the source and $g^{(2)}(0) = 0.50 \pm 0.05$ for light scattered by a single coupler. The on-chip source purity can be estimated considering a signal to noise ratio of about 6 and 2.5 in the two cases, yielding a corrected $g^{(2)}(0)$ equal to 0.11 ± 0.10 and 0.02 ± 0.12 , respectively.

We then analyse the coupling spatial dependence, by recording fluorescence images as a function of the excitation-spot on the sample. Background-subtracted^a counts are then integrated over the three rectangular areas of interest highlighted in Fig.4a around the excitation spot and the two couplers. The results of this procedure are reported e.g. in Fig.4b and d, for a case in which we demonstrate single-molecule-to-WG coupling. Coordinates in the maps correspond to the point of the sample on which pump light is focused, while the fluorescence intensity integrated over one of the three regions of interest is color-coded. The integrated fluorescence map from the excitation point in Fig.4c shows a crystal containing several molecules, out of which only one is coupled to the

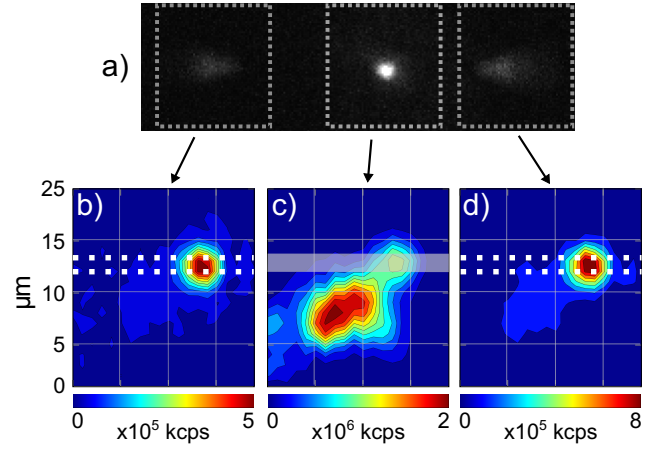


Figure 4: Coupling map. a) EMCCD fluorescence image of the device while exciting a WG-coupled molecule ($\beta \approx 14\%$). b) and d): integrated signal from the coupler areas (dashed white lines in a) as a function of the excitation volume. The corresponding map from the excitation spot is displayed in panel c).

waveguide. This is confirmed by the maps from the coupler areas in panels b and d, showing localized fluorescence. We also observe that residual fluorescence trapped in the anthracene crystal might scatter into the waveguide, giving rise to signal at the outcouplers from otherwise uncoupled molecules. This effect is not hindering the device performances as single molecules are selected by the confocal excitation volume.

A key figure of merit for integrated single photon sources is the branching ratio of the system (β factor), defined as $\beta = \frac{\Gamma_{wg}}{\Gamma_{wg} + \Gamma_{free} + \Gamma_{nr}}$, where Γ_{wg} and Γ_{free} are the radiative decay rate into the waveguide mode and in all other optical modes, respectively, whereas Γ_{nr} accounts for the non-radiative decay rate. Since Γ_{nr} can be to first approximation neglected for DBT:Ac, β is estimated by comparing the fluorescence counts collected on the camera from the coupler areas $C_{c1} + C_{c2} = C_c$ and from the illumination point C_{free} , taking into account the relative collection efficiency (η_i)^b. With these definitions, the branching ratio reads $\beta = \frac{C_c/\eta_c}{C_c/\eta_c + C_{free}/\eta_{free}}$. For light coming from the guided mode, the collection efficiency is solely de-

^aThe background is estimated from areas of the same size right next to each region of interest.

^bBackground subtraction is performed against an average of reference frames, corresponding to positions on the crystal without molecules.

terminated by η_c , as the scattered mode entirely fits within the objective numerical aperture (NA). The collection efficiency for the residual light emitted into free space η_{free} is instead depending on the radiation pattern of the emitter, given the objective NA. We have then evaluated β for each device considering the specifically measured η_c . As for η_{free} , we rely on numerical simulations of two kinds. Maxwell Equations are solved in 3D by means of finite element methods for the geometry outlined in Fig.5a (see SI for details). We devise the anthracene layer of the simplest geometry and with thickness within the experimentally estimated range. We further assume for the refractive indices $n_{\text{Ac}} = 1.8$, $n_{\text{Si}_3\text{N}_4} = 2$ and $n_{\text{glass}} = 1.51$. The DBT molecule is modeled as a Hertzian dipole, placed in an anthracene layer, at a variable distance to the top surface (d) and at the center of the waveguide, with orientation E_x parallel to the only guided mode. In panels b, c, and d we report the electric field norm for a crystal thickness (h) of 100nm and $d = 10\text{nm}$ in three sections of the simulation domain, as marked in the cartoon. η_{free} is calculated as the normalized power flux within a cone of 21° -semiaperture around the dipole polar axis in the collection half space, which corresponds to $\text{NA}=0.55$ after the glass-air interface. This leads to a value of $\eta_{\text{free}} = 5 \pm 1\%$, which is also compatible with the result of semianalytical calculations for the radiation pattern of a Hertzian dipole in a 2D multilayer system representing the sample.¹⁷ The error bar is here estimated by varying the dipole position within the anthracene layer. Using such estimate for η_{free} , we evaluate β from EMCCD images, yielding typical values around $27 \pm 3\%$, with a peak of $40 \pm 3\%$, the error being mostly due to the uncertainty in η_{free} .

The same simulations allow also for an independent estimation of the branching ratio β into the guided mode, as the ratio between the Poynting vector flux through the WG (the detector area being the one depicted in Fig.5d) and the overall radiated power. In Fig.5e we plot the so-calculated β factor as a function of the dipole distance to the waveguide top surface. We conclude that the experimental results are reproduced by the numerical model, where the variability in the branching ratio is accounted for by different possible values for d and h . Finally, lifetime measurements per-

formed on coupled molecules yield values comparable to uncoupled ones within the experimental uncertainty of 10%,³⁸ suggesting that the interaction with the WG only weakly enhances the emission rate. This is again confirmed by numerical calculations of the total radiated power, which results 10% higher when the molecule is in close proximity to the WG. The high β factor should be hence ascribed to a redistribution into the guided mode of the field otherwise propagating at high polar angles in the glass substrate.

In conclusion we have observed, for the first time, single molecule emission into an integrated optical circuit, consisting of a ridge WG terminated with two grating out-couplers. The corrected $g^{(2)}(0) = 0.02 \pm 0.12$ measured from the coupler provides an estimate of the on-chip source purity. Besides on-chip operation, the same device competitively performs also as single photon source into the free-space quasi-gaussian mode of the coupler. In this respect, the source efficiency can be defined as the probability upon excitation to emit a photon into the guided mode, which is then scattered by the grating. It can be then approximately estimated from the measured count rate at the outputcoupler under continuous wave pumping, amounting at best to 10kcounts/s. Assuming for example a saturation parameter of 1/6, considering unitary quantum yield, a detector efficiency of 50%, and experimentally estimating filters and optics transmission to about 5%, the off-chip source efficiency amounts to $\approx 11\%$. This is compatible with our independent estimate of a $40 \pm 3\%$ branching ratio combined with the measured out-coupler efficiency of $40 \pm 1\%$, yielding an overall source efficiency of $16 \pm 2\%$. The slightly higher brightness calculated with respect to photons emitted into free space might be explained e.g. with a small deviation of the quantum yield from 1.

The simplicity of the fabrication process combined with the unique optical properties of the emitter put forward our system as a strong candidate for scalable approaches to on-chip quantum computation. Moreover, a straight-forward extension to many QEs in a single one-dimensional channel could allow the study of manybody effects and quantum correlations.^{26,40} In order to enhance the branching ratio into the WG mode while keep-

ing vanishing on-chip losses, more complex photonic design can be envisioned, compatible with the same fabrication procedure. Replacing an output coupler with a Bragg mirror at the appropriate distance would readily provide a factor 4 improvement,²⁸ whereas practicing a slot in the ridge guide yields a higher field concentration. Finally, we are considering breaking the translational invariance and engineering a higher group index for the same mode area with corrugated-type waveguides,⁴¹ or hybrid photonic crystal ones, yielding high effective photon masses.⁴²

Acknowledgement The authors would like to thank F. Sgrignuoli for helping with numerical simulations, B. Tiribilli, for inspection of the samples by atomic force microscopy, D.S. Wiersma for access to clean room facilities, M. Bellini and C. Corsi for Ti:sapphire operation and Silvia Diewald for help with electron beam lithography. This work benefited from the COST Action MP1403 (Nanoscale Quantum Optics). It is supported by the Erasmus Mundus Doctorate Program Europhotonics (Grant No. 159224-1-2009-1-FR-ERA MUNDUS-EMJD), by the Fondazione Cassa di Risparmio di Firenze (GRANCASSA) and MIUR program Atom-Based Nanotechnology. The authors declare no competing financial interest.

Supporting Information. Details about the optical setup, the sample characterization, the fabrication method and numerical simulations.

References

- (1) O'Brien, J. L.; Furusawa, A.; Vuckovic, J. Photonic quantum technologies. *Nat. Phot.* **2009**, *3*, 687–695.
- (2) Walmsley, I. A. Quantum optics: Science and technology in a new light. *Science* **2015**, *348*, 525–530.
- (3) Knill, E.; Laflamme, R.; Milburn, G. J. A scheme for efficient quantum computation with linear optics. *Nature* **2001**, *409*, 46–52.
- (4) Azuma, K.; Tamaki, K.; Lo, H.-K. All-photonic quantum repeaters. *Nature Communications* **2015**, *6*, 6787–.
- (5) Gatto Monticone, D.; Katamadze, K.; Traina, P.; Moreva, E.; Forneris, J.; Ruo-Berchera, I.; Olivero, P.; Degiovanni, I. P.; Brida, G.; Genovese, M. Beating the Abbe Diffraction Limit in Confocal Microscopy via Nonclassical Photon Statistics. *Phys. Rev. Lett.* **2014**, *113*, 143602.
- (6) Lounis, B.; Moerner, W. E. Single photons on demand from a single molecule at room temperature. *Nature* **2000**, *407*, 491–493.
- (7) Mosley, P. J.; Lundeen, J. S.; Smith, B. J.; Wasylczyk, P.; U'Ren, A. B.; Silberhorn, C.; Walmsley, I. A. Heralded Generation of Ultrafast Single Photons in Pure Quantum States. *Phys. Rev. Lett.* **2008**, *100*, 133601.
- (8) Zumofen, G.; Mojarad, N. M.; Sandoghdar, V.; Agio, M. Perfect Reflection of Light by an Oscillating Dipole. *Phys. Rev. Lett.* **2008**, *101*, 180404–.
- (9) Hwang, J.; Pototschnig, M.; Lettow, R.; Zumofen, G.; Renn, A.; Göttinger, S.; Sandoghdar, V. A single-molecule optical transistor. *Nature* **2009**, *460*, 76–80.
- (10) Somaschi, N. et al. Near-optimal single-photon sources in the solid state. *Nat Photon* **2016**, *10*, 340–345.
- (11) Faraon, A.; Barclay, P. E.; Santori, C.; Fu, K.-M. C.; Beausoleil, R. G. Resonant enhancement of the zero-phonon emission from a colour centre in a diamond cavity. *Nat Photon* **2011**, *5*, 301–305.
- (12) Riedrich-Möller, J.; Arend, C.; Pauly, C.; Mücklich, F.; Fischer, M.; Gsell, S.; Schreck, M.; Becher, C. Deterministic Coupling of a Single Silicon-Vacancy Color Center to a Photonic Crystal Cavity in Diamond. *Nano Lett.* **2014**, *14*, 5281–5287.
- (13) Tiecke, T. G.; Thompson, J. D.; de Leon, N. P.; Liu, L. R.; Vuletic, V.; Lukin, M. D. Nanophotonic quantum phase switch with a single atom. *Nature* **2014**, *508*, 241–244.

- (14) Giesz, V.; Somaschi, N.; Hornecker, G.; Grange, T.; Reznichenko, B.; De Santis, L.; Demory, J.; Gomez, C.; Sagnes, I.; Lemaître, A.; Krebs, O.; Lanzillotti-Kimura, N. D.; Lanco, L.; Auffeves, A.; Senellart, P. Coherent manipulation of a solid-state artificial atom with few photons. *Nature Communications* **2016**, *7*, 11986–.
- (15) Chang, D. E.; Sorensen, A. S.; Demler, E. A.; Lukin, M. D. A single-photon transistor using nanoscale surface plasmons. *Nat Phys* **2007**, *3*, 807–812.
- (16) Curto, A. G.; Volpe, G.; Taminiau, T. H.; Kreuzer, M. P.; Quidant, R.; van Hulst, N. F. Unidirectional Emission of a Quantum Dot Coupled to a Nanoantenna. *Science* **2010**, *329*, 930–933.
- (17) Checcucci, S.; Lombardi, P.; Rizvi, S.; Sgrignuoli, F.; Gruhler, N.; Dieleman, F. B. C.; Cataliotti, F. S.; Pernice, W. H. P.; Agio, M.; Toninelli, C. Planar optical antenna to direct light emission. *Light: Science and Applications* **2016**, *6*, e16245.
- (18) Chu, X.-L.; Brenner, T. J. K.; Chen, X.-W.; Ghosh, Y.; Hollingsworth, J. A.; Sandoghdar, V.; Goetzinger, S. Experimental realization of an optical antenna designed for collecting 99% of photons from a quantum emitter. *Optica* **2014**, *1*, 203–208.
- (19) Hoang, T. B.; Akselrod, G. M.; Mikkelsen, M. H. Ultrafast Room-Temperature Single Photon Emission from Quantum Dots Coupled to Plasmonic Nanocavities. *Nano Lett.* **2015**, *16*(1), 270–275.
- (20) Liebermeister, L.; Petersen, F.; Münchow, A. v.; Burchardt, D.; Hermelbracht, J.; Tashima, T.; Schell, A. W.; Benson, O.; Meinhardt, T.; Krueger, A.; Stiebeiner, A.; Rauschenbeutel, A.; Weinfurter, H.; Weber, M. Tapered fiber coupling of single photons emitted by a deterministically positioned single nitrogen vacancy center. *Applied Physics Letters* **2014**, *104*, 031101.
- (21) Patel, R. N.; Schroder, T.; Wan, N.; Li, L.; Mouradian, S. L.; Chen, E. H.; Englund, D. R. Efficient photon coupling from a diamond nitrogen vacancy center by integration with silica fiber. *Light Sci Appl* **2016**, *5*, e16032–.
- (22) Lodahl, P.; Mahmoodian, S.; Stobbe, S. Interfacing single photons and single quantum dots with photonic nanostructures. *Rev. Mod. Phys.* **2015**, *87*, 347–400.
- (23) Hausmann, B. J. M.; Shields, B.; Quan, Q.; Maletinsky, P.; McCutcheon, M.; Choy, J. T.; Babinec, T. M.; Kubanek, A.; Yacoby, A.; Lukin, M. D.; Lončar, M. Integrated Diamond Networks for Quantum Nanophotonics. *Nano Lett.* **2012**, *12*, 1578–1582.
- (24) Shen, J.-T.; Fan, S. Strongly Correlated Two-Photon Transport in a One-Dimensional Waveguide Coupled to a Two-Level System. *Phys. Rev. Lett.* **2007**, *98*, 153003–.
- (25) Ralph, T. C.; Söllner, I.; Mahmoodian, S.; White, A. G.; Lodahl, P. Photon Sorting, Efficient Bell Measurements, and a Deterministic Controlled-Z Gate Using a Passive Two-Level Nonlinearity. *Phys. Rev. Lett.* **2015**, *114*, 173603.
- (26) Goban, A.; Hung, C.-L.; Hood, J. D.; Yu, S.-P.; Muniz, J. A.; Painter, O.; Kimble, H. J. Superradiance for Atoms Trapped along a Photonic Crystal Waveguide. *Phys. Rev. Lett.* **2015**, *115*, 063601.
- (27) Arcari, M.; Söllner, I.; Javadi, A.; Lindskov Hansen, S.; Mahmoodian, S.; Liu, J.; Thyrrestrup, H.; Lee, E.; Song, J.; Stobbe, S.; Lodahl, P. Near-Unity Coupling Efficiency of a Quantum Emitter to a Photonic Crystal Waveguide. *Phys. Rev. Lett.* **2014**, *113*, 093603–.
- (28) Hwang, J.; Hinds, E. A. Dye molecules as single-photon sources and large optical nonlinearities on a chip. *New Journal of Physics* **2011**, *13*, 085009–.

- (29) Kewes, G.; Schoengen, M.; Neitzke, O.; Lombardi, P.; Schüpfeld, R.-S.; Mazumuto, G.; Schell, A. W.; Probst, J.; Wolters, J.; Lüchel, B.; Toninelli, C.; Benson, O. A realistic fabrication and design concept for quantum gates based on single emitters integrated in plasmonic-dielectric waveguide structures. Scientific Reports **2016**, 6, 28877–.
- (30) Zadeh, I. E.; Elshaari, A. W.; Jüns, K. D.; Fognini, A.; Dalacu, D.; Poole, P. J.; Reimer, M. E.; Zwiller, V. Deterministic Integration of Single Photon Sources in Silicon Based Photonic Circuits. Nano Lett. **2016**, 16, 2289–2294.
- (31) Trebbia, J.-B.; Ruf, H.; Tamarat, P.; Lounis, B. Efficient generation of near infra-red single photons from the zero-phonon line of a single molecule. Opt. Express **2009**, 17, 23986–23991.
- (32) Toninelli, C.; Delley, Y.; Stoferle, T.; Renn, A.; Göttinger, S.; Sandoghdar, V. A scanning microcavity for in situ control of single-molecule emission. Applied Physics Letters **2010**, 97, 021107.
- (33) Faez, S.; Türschmann, P.; Haakh, H. R.; Göttinger, S.; Sandoghdar, V. Coherent Interaction of Light and Single Molecules in a Dielectric Nanoguide. Phys. Rev. Lett. **2014**, 113, 213601.
- (34) Kelkar, H.; Wang, D.; Martín-Cano, D.; Hoffmann, B.; Christiansen, S.; Göttinger, S.; Sandoghdar, V. Sensing Nanoparticles with a Cantilever-Based Scannable Optical Cavity of Low Finesse and Sub- λ^3 Volume. Phys. Rev. Applied **2015**, 4, 054010.
- (35) Ovvy, A. P.; Gruhler, N.; Ferrari, S.; Pernice, W. H. P. Cascaded Mach-Zehnder interferometer tunable filters. Journal of Optics **2016**, 18, 064011.
- (36) Daveau, R. S.; Balram, K. C.; Pregnolato, T.; Liu, J.; Lee, E. H.; Song, J. D.; Verma, V.; Mirin, R.; Nam, S.; Midolo, L.; Stobbe, S.; Srinivasan, K.; Lodahl, P. Efficient fiber-coupled single-photon source based on quantum dots in a photonic-crystal waveguide. arXiv:1610.08670v1 [quant-ph] **2016**,
- (37) Nicolet, A. A. L.; Hofmann, C.; Kol'chenko, M. A.; Kozankiewicz, B.; Orrit, M. Single Dibenzoterrylene Molecules in an Anthracene Crystal: Spectroscopy and Photophysics. ChemPhysChem **2007**, 8, 1215–1220.
- (38) Toninelli, C.; Early, K.; Bremi, J.; Renn, A.; Göttinger, S.; Sandoghdar, V. Near-infrared single-photons from aligned molecules in ultrathin crystalline films at room temperature. Opt. Express **2010**, 18, 6577–6582.
- (39) Ding, Y.; Peucheret, C.; Ou, H.; Yvind, K. Fully etched apodized grating coupler on the SOI platform with 0.58 dB coupling efficiency. Optics letters **2014**, 39, 5348–5350.
- (40) Chang, D. E.; Gritsev, V.; Morigi, G.; Vuletic, V.; Lukin, M. D.; Demler, E. A. Crystallization of strongly interacting photons in a nonlinear optical fibre. Nat Phys **2008**, 4, 884–889.
- (41) Goban, A.; Hung, C.-L.; Yu, S.-P.; Hood, J.; Muniz, J.; Lee, J.; Martin, M.; McClung, A.; Choi, K.; Chang, D.; Painter, O.; Kimble, H. Atom-light interactions in photonic crystals. Nat Commun **2014**, 5, 3808.
- (42) Zang, X.; Yang, J.; Faggiani, R.; Gill, C.; Petrov, P. G.; Hugonin, J.-P.; Vynck, K.; Bernon, S.; Bouyer, P.; Boyer, V.; Lalanne, P. Interaction between Atoms and Slow Light: A Study in Waveguide Design. Phys. Rev. Applied **2016**, 5, 024003.

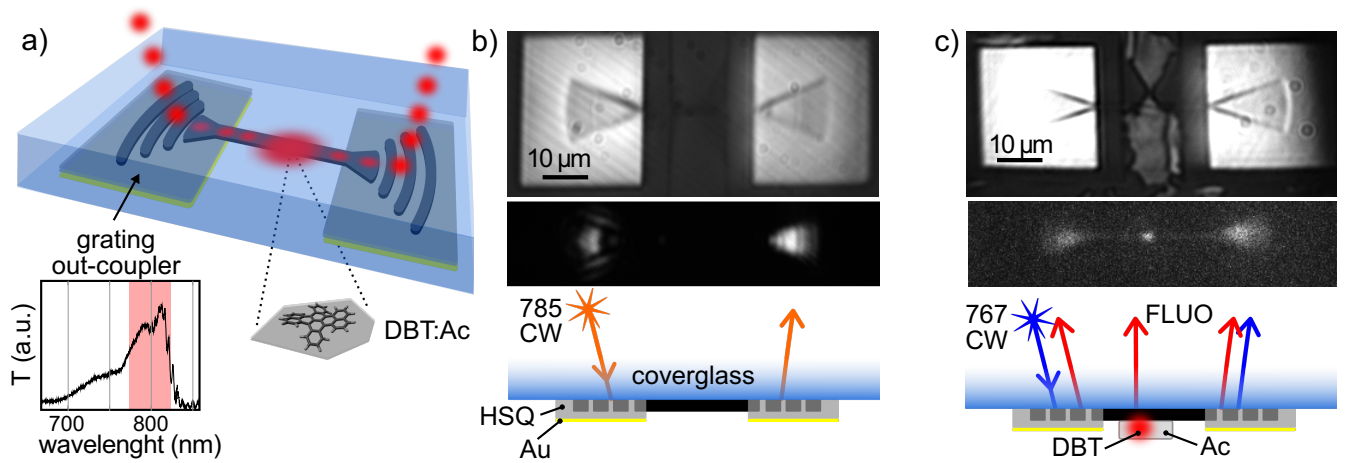


Figure 1: Single-molecule-device working principle. a) Cartoon of the device showing a Si_3N_4 waveguide with two focussing grating outcouplers, coated with an HSQ layer and gold. A single molecule embedded in a thin anthracene crystal laying on top of the bare waveguide region emits a train of guided single photons. In the inset, the grating optical response shows broadband operation around the DBT fluorescence window (red shaded area). In panel b) and c) from bottom to top we report a sketch of the excitation configuration, the resulting signal onto the EMCCD camera and white light images for an empty device (b) and a hybrid molecule-on-waveguide realization (c).

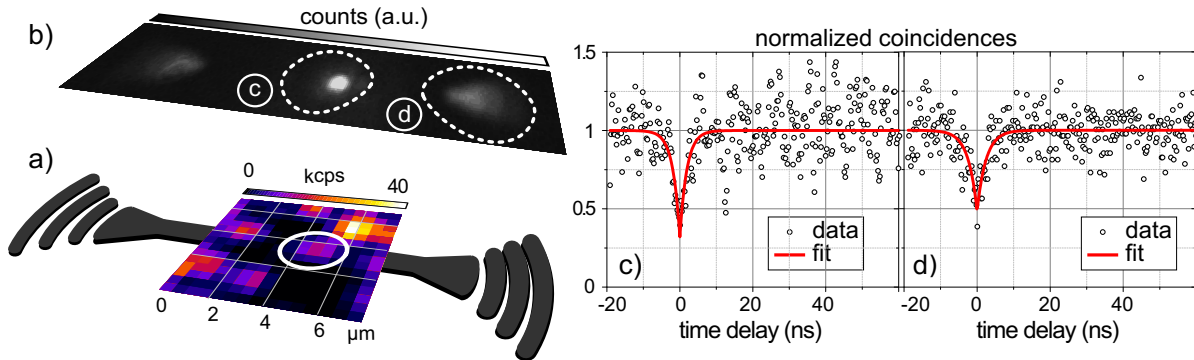


Figure 3: Integrated single photon source. In panel a) a fluorescence confocal scan allows to isolate possibly coupled molecules. The highlighted molecule fluorescence imaged onto the EMCCD camera in b) shows signal at the outcouplers (coupling efficiency $\approx 22\%$). The coupling of single photons into the waveguide finds evidence in the antibunching dip relative to the confocal spot c) and to the coupler area d), respectively.

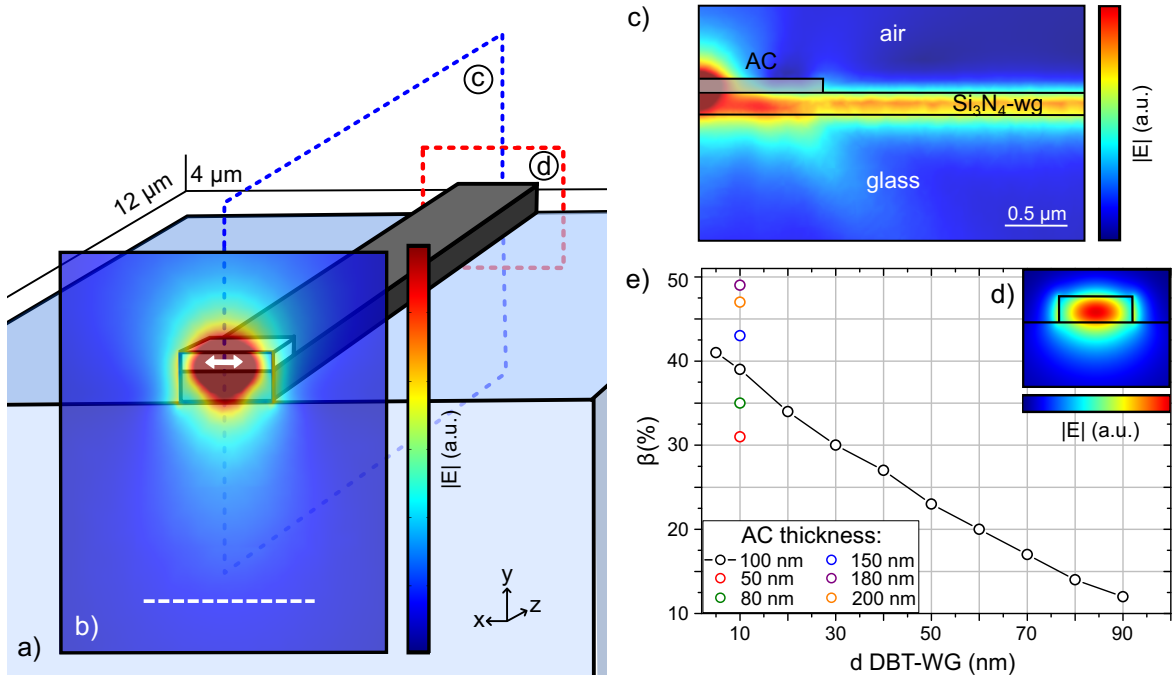


Figure 5: **Numerical simulations.** a) Layout of the 3D numerical simulations displaying half of the waveguide total length (24 μm). A dipolar emitter (white arrow) mimicking a single molecule is placed in a 100 nm-thick anthracene crystal ($n=1.8$). b) Plot of the electric field norm on the plane containing the dipole. The dashed white line represents the objective acceptance angle. Panels c) and d) display the electric field norm in the two respective waveguide sections. In e) the branching ratio for emission into the waveguide mode is reported as a function of the dipole distance to the WG top surface (black dots) and for different crystal thicknesses (colored dots).

Graphical TOC Entry

